

Mapping and modeling of magnetic anomalies in the northern polar region of Mars

L. L. Hood

Lunar and Planetary Laboratory, University of Arizona, Tucson, Arizona

A. Zakharian

Lunar and Planetary Laboratory, University of Arizona, Tucson, Arizona

Arizona Center for Mathematical Sciences, University of Arizona, Tucson, Arizona

Abstract. Vector crustal magnetic field maps of the northern polar zone (60°N to 90°N) are constructed from selected Mars Global Surveyor magnetometer data obtained during the period from May 28 to September 13, 1998. Two medium anomalies (amplitudes >50 nT at 170 km altitude) are mapped in locations consistent with earlier studies. No visible surface features correlate with the anomalies, suggesting that the sources lie beneath the visible veneer of polar deposits and volcanic lava flows. If so, then they formed prior to the immediate end of the heavy bombardment (upper Hesperian) period. Modeling of anomaly vector field components combined with independent constraints on the depth to the Curie isotherm yields lower limits on bulk magnetization intensities (0.4 – 0.9 A/m) that are significantly greater than those measured for Martian (SNC) meteorite samples. Rocks that contain substantially more titanomagnetite than SNC meteorites, or that contain magnetic phases in addition to titanomagnetite, possibly resulting from hydrothermal alteration, are therefore suggested. Alternatively, remanence acquisition in a field of Earthlike intensity ($\sim 50 \mu\text{T}$), rather than in the relatively weak inferred paleointensities for SNC meteorites ($\sim 1 - 10 \mu\text{T}$), would also help to explain the relatively strong inferred remanent magnetizations. The approximate south paleomagnetic pole positions corresponding to these two anomaly sources are located in a region between Olympus Mons and the present north rotational pole. This region is adjacent to the approximate location predicted by *Melosh* [1980] for the paleopole prior to the formation of the Tharsis gravity anomaly.

1. Introduction

Although Mars has no intrinsic global magnetic field at present, the magnetometer on the Mars Global Surveyor (MGS) spacecraft detected crustal magnetic field anomalies with amplitudes as large as 400 nT (1 nT = 10^{-5} G) at 110 km altitude [*Acuña et al.*, 1998, 1999; *Connerney et al.*, 1999]. Interpretation of the observed crustal fields is constrained by studies of shergotite, nakhlite, and chassignite (SNC) meteorites and surface magnetometer data which show that the dominant remanence carriers in Martian crustal rocks are iron oxides [*Hargraves et al.*, 1977; *Collinson*, 1986; *Cisowski*, 1986]. Remanence carriers of this type (e.g., titanomagnetite, maghemite) would have acquired their magnetizations over significant time periods. For example, a massive igneous intrusion containing magnetite would

have cooled only gradually over millions of years. Such extended periods of magnetization acquisition would necessarily require the continual presence of a steady, unidirectional magnetizing field. In addition, the observed anomalies tend to be most numerous over older (Noachian and Hesperian) terrain, suggesting that the Martian magnetizing field existed mainly during the period prior to the end of the early heavy bombardment of Mars [*Acuña et al.*, 1999].

By analogy with the terrestrial case, the most probable source of a steady magnetic field early in Mars' history would have been a core dynamo. Consistent with this interpretation, thermal history models admit the possibility that a core dynamo could have existed early (during the first gigayear) of Mars' history [*Stevenson et al.*, 1983; *Schubert and Spohn*, 1990]. Specifically, isotopic constraints from SNC meteorites imply that formation of a metallic core in Mars must have occurred early, shortly after accretion, and most thermal models indicate that the core would have been fluid and convectively unstable for a substantial period (>0.5 Gyr). The

Copyright 2001 by the American Geophysical Union.

Paper number 2000JE001304.
0148-0227/01/2000JE001304\$09.00

absence of an intrinsic field during the present epoch is attributable to cooling of the core to a subadiabatic, conductive state combined with the absence of a freezing inner core that would have driven chemical convection. The latter condition is met if the sulfur abundance in the core is greater than ~ 15 wt % [Stevenson *et al.*, 1983]. Some recent models have argued that the cessation of dynamo generation may have been governed by the presence or absence of plate tectonics or some other process that causes rapid surface heat flux [Nimmo and Stevenson, 2000].

If the magnetization of major crustal anomaly sources on Mars was due to the presence of a former core dynamo, then the bulk directions of magnetization of these sources should reflect the orientation of the planetary magnetic field at the times of their formations. Assuming that the dynamo magnetic moment vector was roughly constant in orientation (aside from reversals), it follows that the corresponding magnetic pole positions for anomaly sources of similar ages should ideally be in the same areographic region(s). Thus analysis of the MGS magnetometer data to infer bulk directions of magnetization of major anomaly sources could provide a direct test of the core dynamo hypothesis. Moreover, if the areographic region(s) in which former magnetic pole positions are found is displaced significantly from the present rotational polar zone, this displacement could represent evidence for reorientation of the planet relative to its spin axis ("polar wandering"). The latter application assumes that the former dynamo moment vector was approximately aligned with the planetary rotation vector, a condition that is met for most observed planetary fields, including that of the Earth [e.g., Russell, 1987].

It should be noted that the interpretation of Martian crustal magnetic fields as being a consequence of thermoremanence or chemical remanence in a former core dynamo magnetic field neglects any contributions from impact processes to the observed crustal paleomagnetism. On the Moon, there is evidence that impact processes have played a substantial role both in producing the materials that are magnetized and in modifying any preexisting magnetic field such as a former core dynamo field (for reviews of lunar paleomagnetism studies, see Hood [1995] and Fuller and Cisowski [1987]). This is partly because the dominant ferromagnetic carriers in the reducing lunar environment are microscopic metallic iron particles that typically originate by impact shock reduction of preexisting ferromagnesian silicates. These carriers are embedded in surficial materials that could have acquired their magnetizations relatively quickly (by shock or rapid cooling). In addition, hypervelocity impacts on planetary surfaces vaporize silicate materials, resulting in a hot, partially ionized, thermally expanding plasma cloud at the impact point [Hide, 1972; Hood and Vickery, 1984]. These expanding impact plasma clouds interact strongly with ambient magnetic fields, producing transient fields ca-

pable of magnetizing lunar materials. However, at Mars the presence of a denser, oxidizing atmosphere during the period when a core dynamo existed would have minimized the contribution of impact plasmas to the observed paleomagnetism. The fact that Martian crustal field anomalies are several orders of magnitude stronger than lunar anomalies at the same altitude is consistent with larger volumes and therefore slower formation times for anomaly sources. Thus, except possibly for impact demagnetization of crustal regions during large basin-forming impacts, it appears reasonable to consider primarily a "terrestrial model" in which the paleomagnetism originated by relatively slow internal crustal processes in the presence of a steady core dynamo magnetic field.

In this paper an analysis is presented of original MGS magnetometer data delivered so far (as of June 2000) to the Planetary Data System for general use by the planetary science community. These data were obtained during the period from May 28 to September 13, 1998 (MGS orbits 327 to 553) and are from a period in the MGS mission known as Science Phasing Orbits (SPO) 1 and 2. Data coverage is limited to the northern polar region (60°N to 90°N). Although two major medium-amplitude (~ 50 nT) anomalies have previously been mapped in this region [see Acuña *et al.*, [1999, Figure 1], the earlier mapping procedure involved averaging all available measurements over altitude (170-200 km). In section 2 the methods adopted to process and map the vector components of the crustal field in the work reported here are described. In particular, only a selected subset of available data over a given region is used in order to avoid averaging over altitude. In section 3, source characteristics for the two major mapped anomalies are investigated using a simplified, iterative forward modeling procedure. Specifically, limits on bulk magnetization intensities, directions of magnetization, and corresponding magnetic pole positions for a former magnetizing dipole centered in Mars are estimated for these two anomaly sources. In section 4 the interpretation and implications of the modeling results are discussed, while conclusions are given in section 5.

2. Data Processing and Mapping

For the purpose of constructing regional maps of Martian crustal magnetic fields, we applied a modified version of methods developed for mapping lunar crustal magnetic fields using Apollo subsatellite magnetometer data [Hood *et al.*, 1981] and Lunar Prospector magnetometer data [Hood *et al.*, 2001]. However, one major difference between the lunar case and the Martian case is the presence of a Martian ionosphere whose electron density reaches a maximum at altitudes between about 180 and 210 km [Acuña *et al.*, 1998]. In the lunar case, under at least some conditions, crustal fields can be mapped in a quasi-vacuum environment at all altitudes with minimal external field disturbances. However, at

Mars, at altitudes equal to or greater than the ionospheric peak, strong and variable magnetic fields associated with the solar wind-ionosphere interaction are commonly present. These external field disturbances greatly increase the difficulty of detecting and mapping permanent crustal fields when the spacecraft is at or above the ionospheric peak.

A second difference between the Martian case and the lunar case is the much larger longitudinal separation between successive orbit tracks for MGS as compared to lunar orbiting spacecraft. Because of the relatively slow lunar rotation rate, lunar polar orbit tracks are separated by ~ 30 km at the equator. This allows a relatively easy comparison of field measurements on successive orbits to distinguish permanent crustal fields from transient external fields. At Mars a minimum spacecraft orbit period of ~ 1.9 hours combined with the planetary rotation period of 24.6 hours leads to a minimum longitudinal orbit spacing at the equator of $\sim 28^\circ$, or ~ 1650 km. The spacing is wider for longer-period, elliptical orbits. Such a large orbit spacing precludes measurements of the same magnetic anomaly fields on successive orbits. Hence a more complex procedure of sorting periapsis passes according to longitude and altitude is necessary before comparisons of adjacent orbit passes can be attempted.

Taking into account the above noted differences between the Martian and lunar measurement environments, the following general processing steps were applied to the MGS magnetometer data. (1) Selection of all available orbit segments during which the spacecraft altitude is less than that of the ionosphere electron density peak (conservatively taken to be 200 km). (2) Transformation of field data to a spherical polar radial, east, and north coordinate system followed by merger with ephemeris data to produce a file containing the field components, spacecraft (S/C) altitude, longitude, latitude, and a flag to identify day or night conditions. (3) Ordering of orbit segments according to spatial location so that successive orbits are adjacent to one another. (4) Visual editing of periapsis passes by comparison of measurements on adjacent passes to eliminate intervals with significant external magnetic field disturbances. (The radial field component is examined first because the tangential components (east, north) tend to be more disturbed by external fields.) (5) Filtering of remaining orbit segments by quadratic or higher-order polynomial detrending. (This step further assists in minimizing long-wavelength external field variations.) (6) Two-dimensional filtering (or gridding) of individual orbit data segments to produce an equally spaced array of measurements along the (curved) surface defined by the mean S/C altitude. (Maps of the three field components (radial, east, and north), of the field magnitude, of the S/C altitude (radial distance from the center of figure minus the mean planetary radius), and of the orbit track locations are also produced at

this stage. Software for this purpose is based on algorithms originally developed by *Ehason and Soderblom* [1977] for the analysis of Apollo subsatellite data sets.)

An examination of the 226 orbits of MGS magnetometer data available for analysis at present (June 2000) showed that the region north of 60°N latitude was covered multiple times at variable altitudes. It was therefore decided to divide the data set into subsets with each subset containing a sequence of orbits with nearly single-altitude coverage as a function of position.

One sequence of orbits (438-495; July 20 to August 17, 1998) was found to provide a general overview of the northern polar region from 60°N to 88°N . The resulting maps of the field magnitude, the radial, east, and north components, the S/C altitude, and orbit track locations are shown in Plate 1. The mean altitude structure (bottom left plot) is nearly symmetric about the north pole with a minimum altitude of ~ 163 km near 75°N . Two major anomalies are evident on the field magnitude plot (top left). The radial field component plot (top right) agrees approximately with that published earlier by *Acuña et al.* [1999] (see their Figure 1). These anomalies, centered near 83°N , 32°E and near 65°N , 27°E , will be referred to hereafter as the northern and southern anomalies, respectively.

In order to produce the best possible map of each of the major anomalies of Plate 1, it is desirable to select those orbit passes that cover each anomaly at the lowest available altitudes with a minimum of external field disturbances. For the purpose of producing an optimal map of the southern anomaly, orbits 496-553 (August 17 to September 13, 1998) were selected. These orbits have periapses that are centered near 65°N , which is the approximate latitude of the southern anomaly. Figure 1a shows six tracks chosen from among this group because of their location over the region occupied by the southern anomaly. Figures 1b, 1c, and 1d are plots of the radial, east, and north field components, respectively, for this series of six orbits. The repetition of patterns on successive orbits verifies that external transient fields are relatively small.

Figure 2 is a regional field map covering the area occupied by the southern anomaly. It was constructed from a subset of orbits 496 to 553, including the six orbits selected for Figures 1a-1d. Although parts of only 10 orbits were used, it represents an optimally accurate map at the lowest available altitude of observation over this region.

For the purpose of producing an optimal map of the northern anomaly, orbits 327-437 (May 28 to July 20, 1998) were selected. These orbits have mean periapses of ~ 165 km at latitudes near 83°N and are therefore positioned well for detecting this anomaly. Figure 3a shows a series of eight tracks located over the region occupied by the anomaly. Figures 3b, 3c, and 3d are plots of the radial, east, and north field components, respectively, for this series of six orbits in the same format as

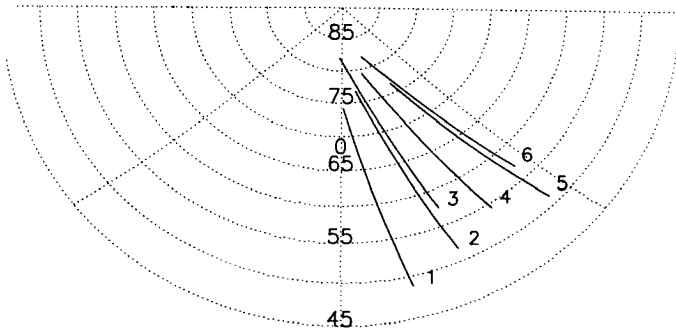


Figure 1a. Surface tracks selected from orbits 496-553 (August 17 to September 13, 1998) for coverage over the southern field anomaly of Plate 1.

Figures 1b, 1c, and 1d. The repetition of field patterns again verifies that the measured fields are dominantly crustal in origin.

Figure 4 is a regional map covering the northern anomaly region constructed from a subset of orbits 327-437, including the eight orbits examined in Figures 3a-3d. To produce this map, >40 orbit segments were used. Although the field component patterns in Figures 2 and 4 are similar in many respects to those shown in the larger-scale map of Plate 1, the lower altitudes and improved selection of the data used in Figures 2 and 4 result in more accurate maps for modeling purposes.

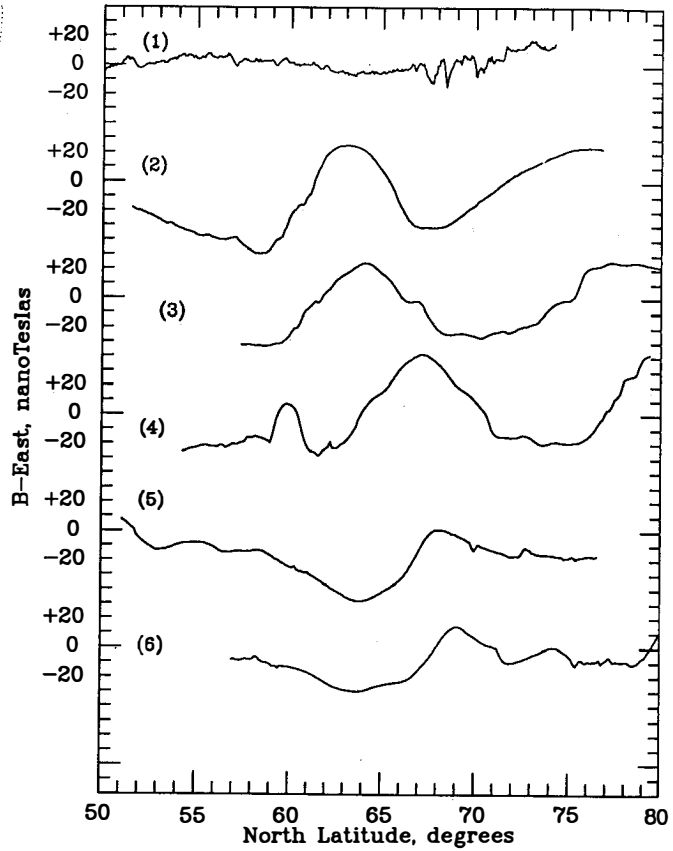


Figure 1c. Same format as Figure 1b but for the east field component.

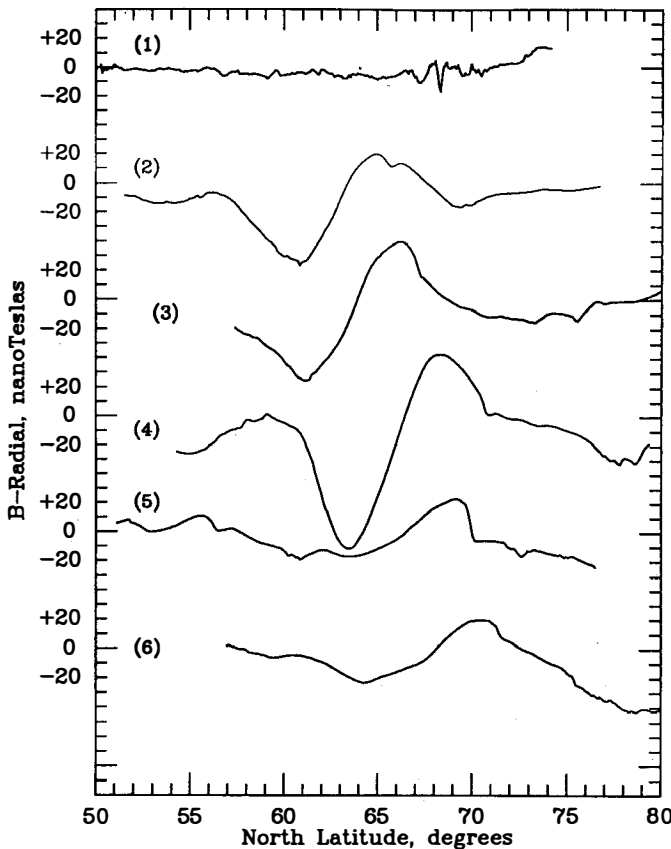


Figure 1b. Plots of the radial magnetic field component along the series of surface tracks shown in Figure 1a. The numerical labels identify the tracks.

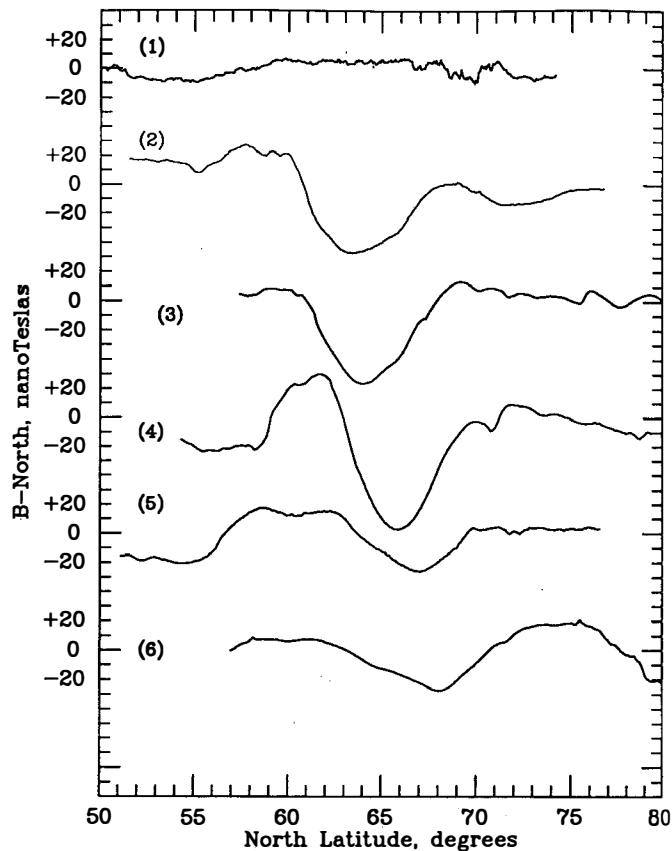


Figure 1d. Same format as Figure 1b but for the north field component.

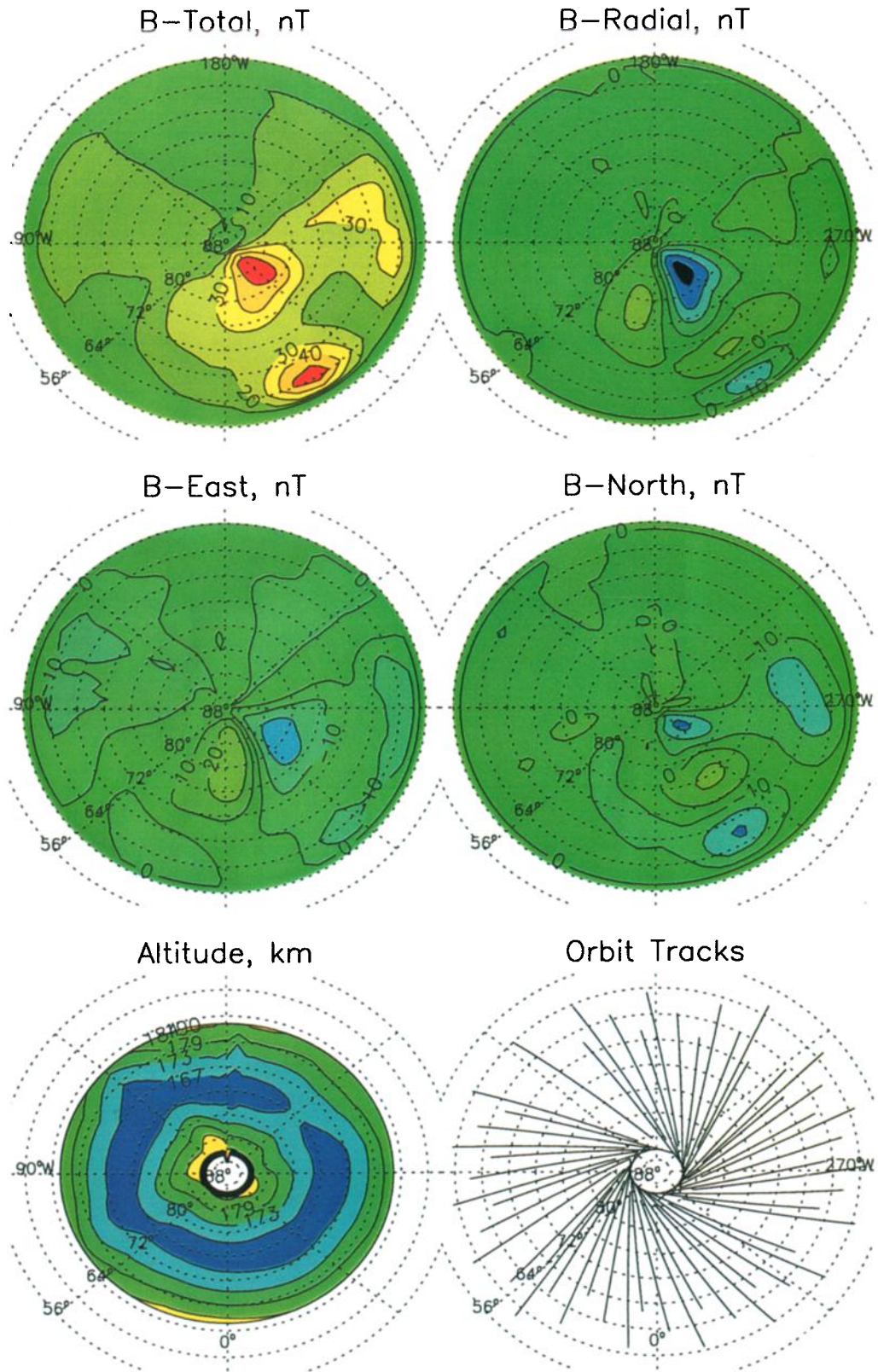


Plate 1. Maps of the field magnitude, the radial, east, and north field components, the spacecraft altitude, and the orbit track locations produced for orbits 438-495 (July 20 to August 17, 1998). The effective latitudinal coverage is 60°N to 90°N.

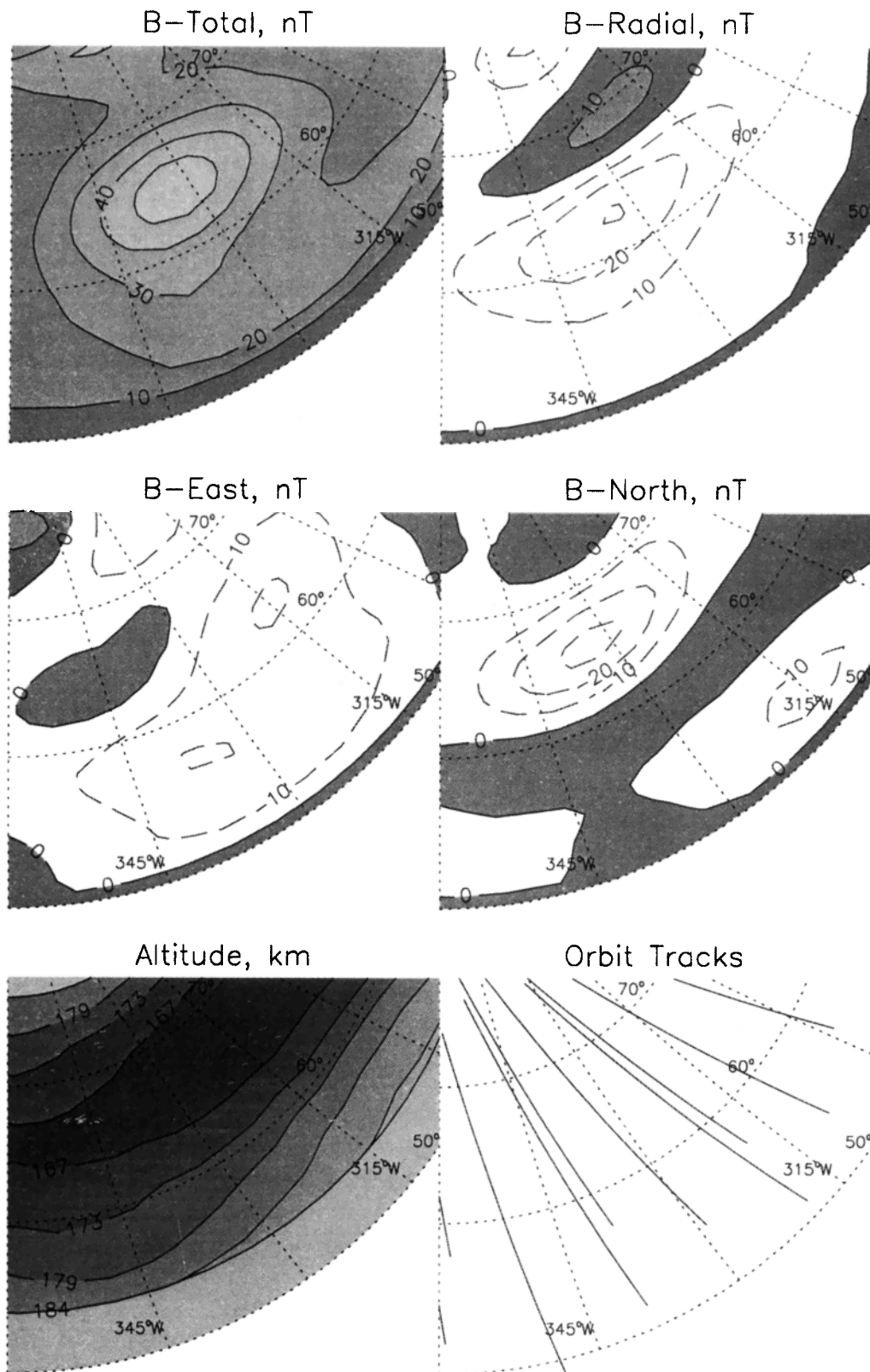


Figure 2. Regional vector field map of the southern anomaly of Plate 1 constructed from a subset of orbits 496-553 (August 17 to September 13, 1998). The field magnitude, mean spacecraft altitude, and orbit track distribution are also shown.

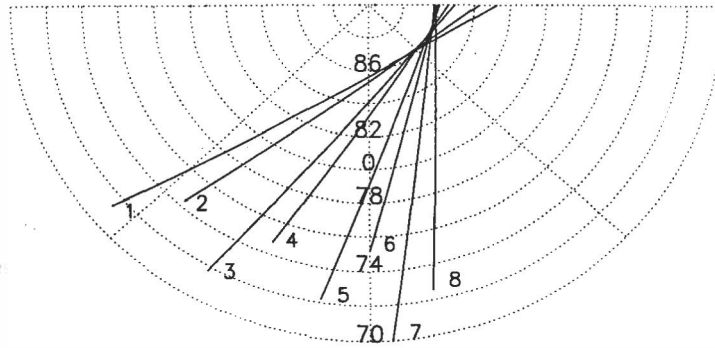


Figure 3a. Surface tracks selected from orbits 327-437 (May 28 to July 20, 1998) for coverage over the northern field anomaly of Plate 1.

3. Model Calculations

In order to investigate possible source characteristics for the northern and southern anomalies of Figures 2 and 4, we have employed an approximate, iterative forward modeling procedure [see, e.g., Hood, 1980]. Since the two mapped anomalies are relatively isolated and are dominantly dipolar, we assume that a single source is responsible for each. For simplicity, two extreme end-member source model geometries were investigated: (1)

a point dipole with moment amplitude m buried at a depth d and (2) a circular surface disk with dipole moment per unit area \bar{m} and diameter D . An improved fit to the data could be obtained using more than one dipole or using a surface disk of arbitrary shape; however, for the purpose of the present first-order analysis a single dipole or a circular disk is employed. The orientation of the dipole moment vector and that of the magnetization vector in the disk are both described by two angles, α and β , where α is the angle between the local radial direction and the moment vector and β is the azimuth of the surface projection of the mo-

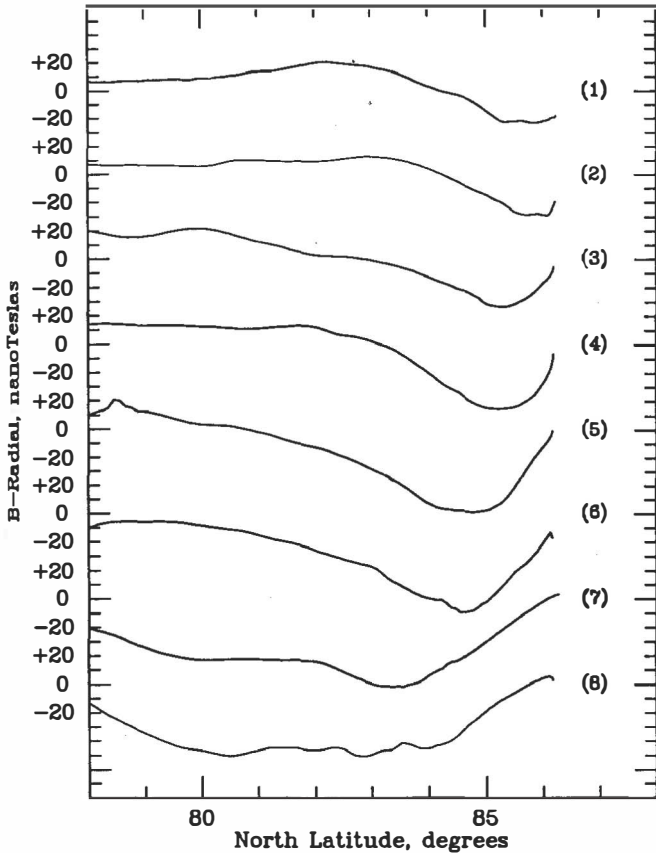


Figure 3b. Plots of the radial magnetic field component along the series of surface tracks shown in Figure 3a. The numerical labels correspond to the tracks in Figure 3a.

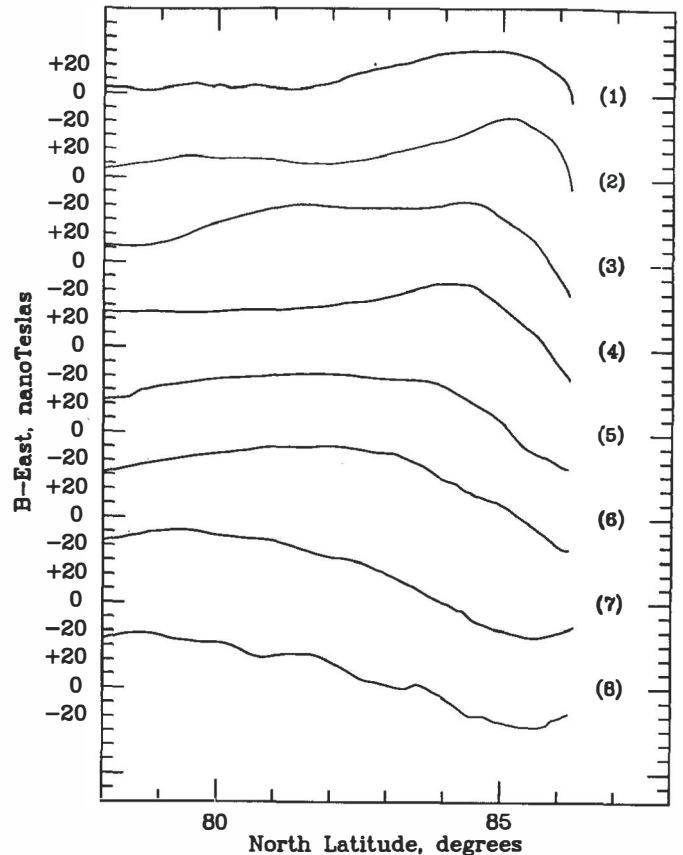


Figure 3c. Same format as Figure 3b but for the east field component.

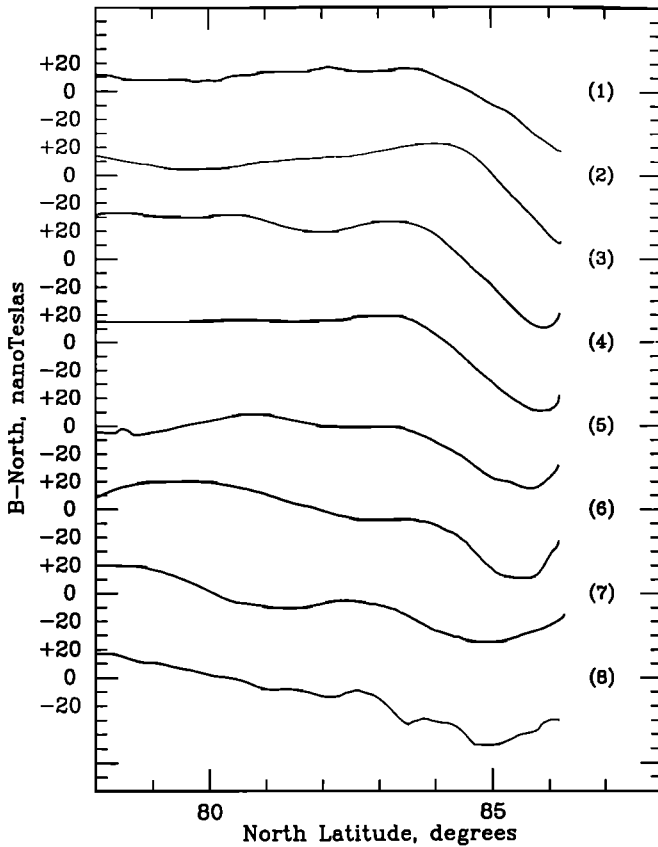


Figure 3d. Same format as Figure 3b but for the north field component.

ment vector measured from the local eastward direction counterclockwise (looking down) about the radial direction. These angles are easily relatable to the conventional angles of terrestrial paleomagnetism, I and D [see, e.g., *Butler, 1992; Langel and Hinze, 1998*]. As indicated schematically in Figure 5, each of these two source models, with suitably chosen parameters, will produce a nearly identical field at the S/C altitude. Therefore field measurements at a single altitude will not uniquely distinguish between these source models. Nevertheless, an evaluation of source model parameters combined with additional physical constraints (depth to the Curie isotherm, likely geologic nature of anomaly sources) can yield limits on bulk magnetization intensities. In addition, as also indicated schematically in Figure 5, the inferred orientation of the buried dipole moment vector and the magnetization direction in the surface disk are approximately equal. Thus the derived direction of magnetization is not strongly sensitive to assumed source model geometry.

Initially, iterative forward model calculations were performed for both anomalies assuming a buried point dipole source geometry. The modeling procedure consisted of first placing the dipole at the longitude and latitude where the field magnitude reached a maximum amplitude and at an arbitrary depth. The direction angles α and β were also set at values roughly consistent

with the observed field component patterns. Then, both the dipole moment amplitude \mathbf{m} and the depth d were iteratively varied until a fitting parameter measuring the deviation of the model field components from the observed field components and the model field magnitude from the observed field magnitude reached a minimum. In order to increase sensitivity to fields associated directly with the anomaly, the fitting parameter calculation was performed only within a small area centered on the anomaly. The calculation was then repeated with \mathbf{m} and d held constant and the direction angles α and β determined by the fitting procedure. This process was repeated cyclically until no significant change in the fitted parameters (\mathbf{m} , d , α , and β) occurred.

Following *Butler [1992]*, once the source surface location and direction of magnetization were estimated, the corresponding magnetic pole position location was determined using the following series of steps: First, the great-circle distance from the anomaly site to the magnetic pole, the magnetic colatitude p , was obtained from

$$p = \tan^{-1}(-2 \tan \alpha). \quad (1)$$

The pole latitude was then given by

$$\lambda_p = \sin^{-1}(\sin \lambda_s \cos p + \cos \lambda_s \sin p \sin \beta), \quad (2)$$

where λ_s is the source surface latitude. The longitudinal difference between pole and site is positive toward the east and was obtained from

$$\Delta\phi = \sin^{-1}\left(\frac{\sin p \cos \beta}{\cos \lambda_p}\right). \quad (3)$$

If $\cos p \geq \sin \lambda_s \sin \lambda_p$, then the pole longitude was given by $\phi_p = \phi_s + \Delta\phi$, where ϕ_s is the source surface longitude. Otherwise, $\phi_p = \phi_s + 180^\circ - \Delta\phi$.

In order to estimate the approximate errors associated with a given pole position location, we assume that any model-derived bulk direction of magnetization is characterized by a circular error cone of angular radius δ_{95} . Again following *Butler [1992]*, this circular confidence limit about the direction of magnetization at the source may be mapped into an ellipse of confidence about the pole position. The semiaxis of this ellipse along the great circle from the source to the paleopole is

$$dp = \delta_{95} \left(\frac{1 + 3 \cos^2 p}{2} \right). \quad (4)$$

The semiaxis perpendicular to this great circle is

$$dm = \delta_{95} \left(\frac{\sin p}{\sin \alpha} \right). \quad (5)$$

In the case of the southern anomaly an optimal fit to the observed field was obtained for a location at 65°N , 27°E ; direction angles $\alpha = 115^\circ \pm 20^\circ$ and $\beta = 100^\circ \pm 20^\circ$; moment $\mathbf{m} = 2.4 \pm 0.4 \times 10^{16} \text{ A m}^2$ ($= 2.4 \pm 0.4 \times 10^{19} \text{ G/cm}^3$); and depth $d = 160 \pm 40 \text{ km}$. The corresponding south magnetic pole position is at approximately 38°N , 141°W , with error ellipse semiaxes

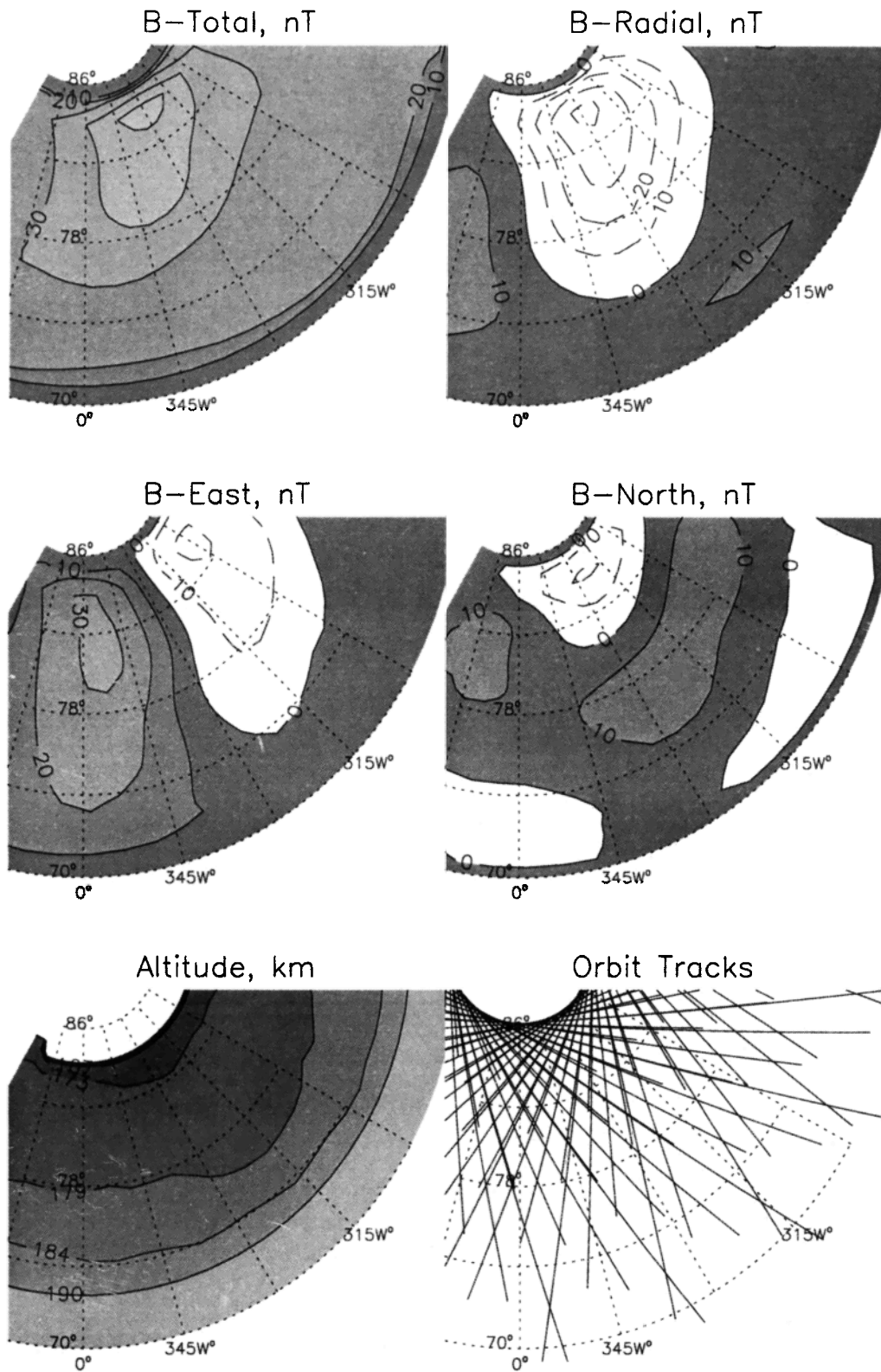


Figure 4. Regional vector field map of the northern anomaly of Plate 1 in the same format as Figure 2. This map was constructed from a subset of orbits 327-437 (May 28 to July 20, 1998).

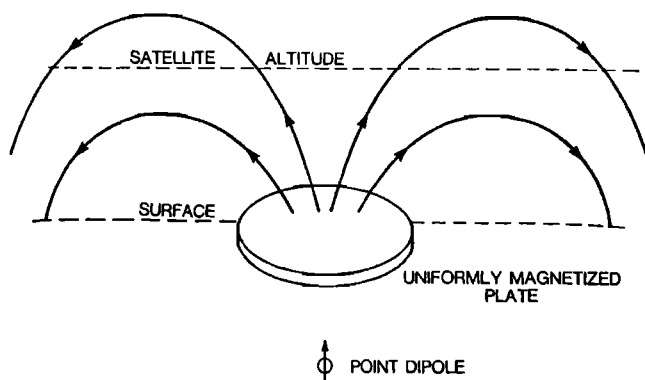


Figure 5. Two possible source models for an isolated, dominantly dipolar crustal magnetic field anomaly. See the text.

of $dp = 12^\circ$ and $dm = 21^\circ$. The north magnetic pole position is antipodal to this location and lies in the southern hemisphere. In the case of the northern anomaly an optimal fit was obtained for a location at 83°N , 32°E ; direction angles $\alpha = 160^\circ \pm 20^\circ$ and $\beta = 100^\circ \pm 20^\circ$; moment $\mathbf{m} = 1.2 \pm 0.3 \times 10^{16}$ A m² ($= 1.2 \pm 0.3 \times 10^{19}$ G/cm³); and depth $d = 150 \pm 40$ km. The corresponding south magnetic pole position lies at approximately 61°N , 136°W with error ellipse semiaxes of $dp = 30^\circ$ and $dm = 15^\circ$.

Figure 6a is a plot of the fitting parameter versus the angle α for the southern anomaly point dipole model with all other parameters held constant. For values of α less than $\sim 95^\circ$ or more than $\sim 135^\circ$, the fitting parameter increases to significantly more than its minimum value at approximately $\alpha = 115^\circ$. On this basis an error range of $\pm 20^\circ$ was adopted. Figure 6b is a similar plot of the fitting parameter versus β for the southern anomaly point dipole model. Again, the fitting parameter increases to significantly more than its minimum value at $\sim 20^\circ$ more or less than the minimum near $\beta = 100^\circ$. As shown in Figures 6c and 6d, an approximate $\pm 20^\circ$ error range for α and β for the northern anomaly is also suggested. Similar plots of fitting parameter versus moment amplitude and depth were used to estimate error ranges for dipole moment amplitude and depth.

Next, iterative forward model calculations were performed for both anomalies, assuming a thin surface disk source geometry. The modeling procedure was the same as that described above for a point dipole source model except that the dipole moment per unit area \mathbf{m}/area and the disk diameter D were determined in place of the point dipole moment and depth. In the case of the southern anomaly, the fitted dipole moment per unit area $\mathbf{m}/\text{area} = 9.2 \pm 1.4 \times 10^4$ A ($= 9200 \pm 1400$ G-cm), while the estimated diameter D is 360 ± 70 km. For the northern anomaly the corresponding values are $\mathbf{m}/\text{area} = 4.2 \pm 2.0 \times 10^4$ A (4200 ± 2000 G-cm) and $D = 400 \pm 60$ km. The surface locations and directions of magnetization were unchanged from the point dipole source results.

Figure 7 is a comparison of the observed southern anomaly fields (from Figure 2) with the surface disk model fields for the best fitting parameters listed above. Figure 8 is a similar comparison for the northern anomaly. As can be seen, the model fields do simulate the general character of the three field components and the field magnitude in both cases.

4. Interpretation and Implications

4.1. Anomaly Sources and Magnetic Phases

The northern anomaly (83°N , 32°E) is located over the young Planum Boreum polar plateau of layered deposits and ice, while the southern anomaly (65°N , 27°E) occurs over an undistinguished portion of upper Hesperian-aged north polar plains (Vastitas Borealis). The latter unit consists of degraded lava flows or sediments punctuated by small knobby volcanoes and degraded highland material [Tanaka and Scott, 1987]. However, there is no visible surface feature where the anomalies are located. Both the polar layered deposits and the polar plains lava flows are relatively surficial

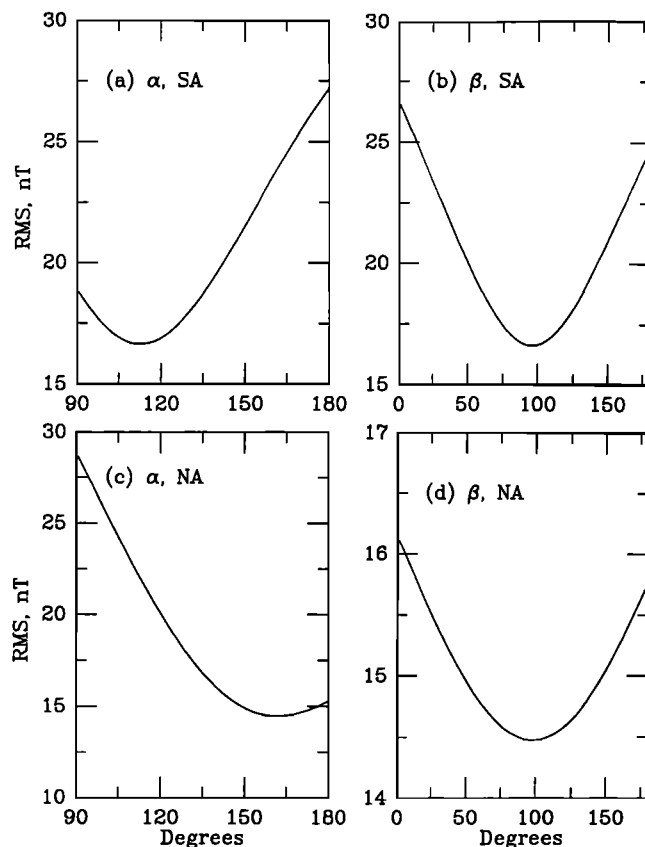


Figure 6. (a) Plot of the fitting parameter (analogous to the root mean square deviation, or RMS) in nT as a function of the angle α for the southern anomaly model dipole moment vector orientation; (b) same format as Figure 6a but for the angle β (southern anomaly case); (c) same format as Figure 6a but for the northern anomaly model dipole moment vector orientation; and (d) same format as Figure 6a but for the angle β (northern anomaly case).

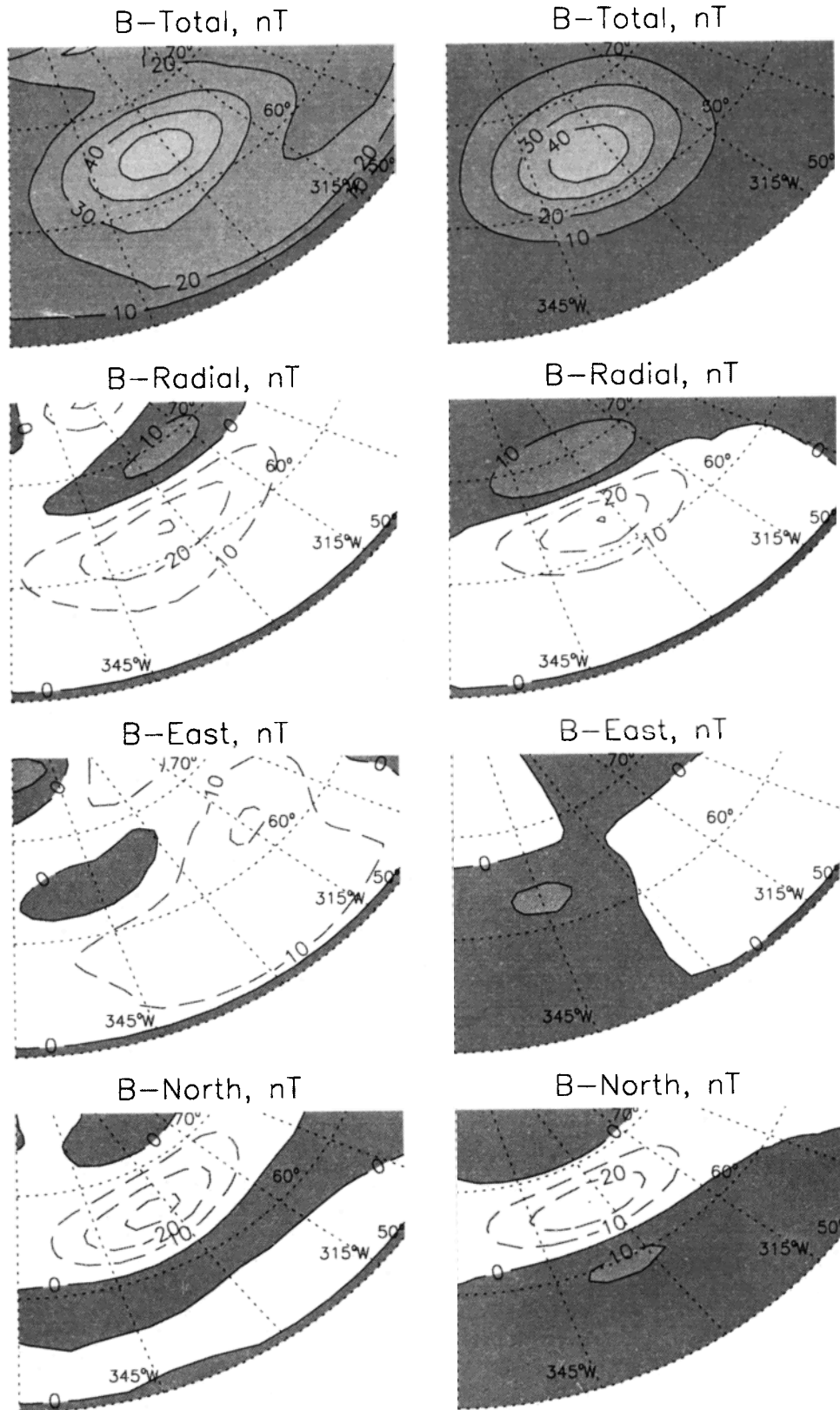


Figure 7. Comparison of the field magnitude and vector field components calculated using a surface disk source model (right panels) to those calculated from the MGS magnetometer data for the southern anomaly of Plate 1. See the text for disk model parameters.

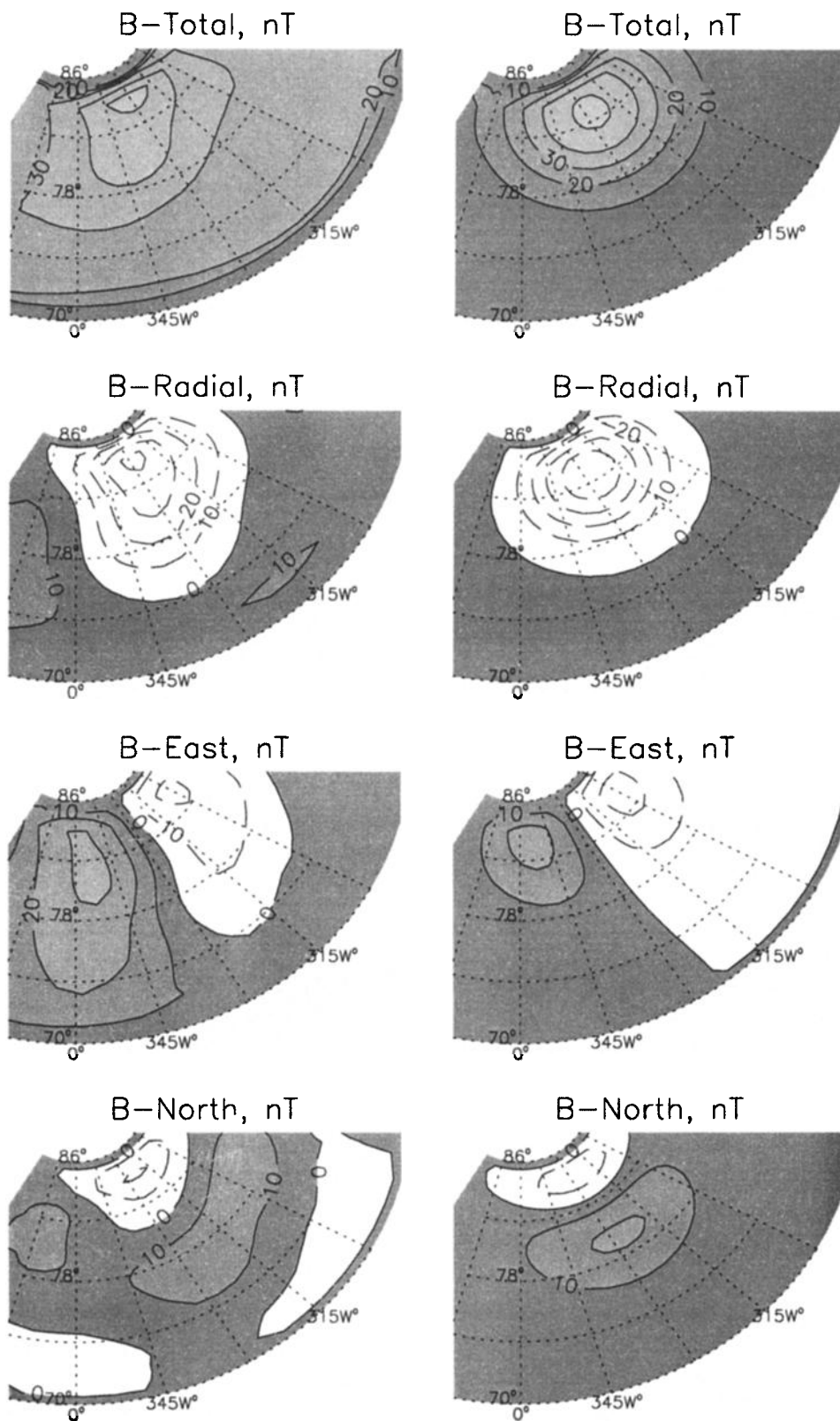


Figure 8. Same format as Figure 7 but for the northern anomaly of Plate 1. See the text for disk model parameters.

and are roughly symmetric about the pole. The sources of these anomalies are therefore most probably beneath the visible surface. As shown in Plate 2, there are no gravity or topographic anomalies that correlate clearly with these magnetic anomalies. It is therefore unlikely that a significantly denser subsurface body is responsible for either anomaly. In some areas, such as Phlegra Montes and Acidalia Planitia, plains units surround and embay eroded and hilly terrain that resembles material from the southern highlands. Martian crustal anomalies are generally stronger south of the dichotomy boundary separating the northern low plains from the southern highlands [Acuña *et al.*, 1999]. Therefore it might be suggested that the sources of the northern polar anomalies studied here are older highlands units beneath the visible surface. However, the lack of association of magnetic anomalies with visible eroded and hilly terrain indicates that the magnetization of these units must be rather inhomogeneous.

Because of their locations within the northern lowlands, any complete discussion of the origins of the anomalies analyzed here must consider also the origin of the crustal dichotomy on Mars. One hypothesis for the origin of the dichotomy involves one or more giant basin-forming impacts in the northern region, followed by volcanic lava flooding and erosion [Wilhelms and Squyres, 1984; Frey and Schultz, 1988; Strom *et al.*, 1992]. According to this hypothesis, the northern lowlands would be similar in origin to the extensive maria on the lunar nearside [see Tanaka *et al.*, 1992, Figure 1]. Alternatively, Wise *et al.* [1979] suggested that a single mantle convection cell eroded the lower crust in what is now the northern zone of Mars; the lowland plains are then suggested to have resulted from subsequent foundering of the upper crust and later lava flooding and erosion [see also McGill and Dimitriou, 1990]. Recent interpretations of MGS topography and gravity data cast doubt on the impact model of the crustal dichotomy [Zuber *et al.*, 2000], leaving tectonic subcrustal erosion as the currently favored hypothesis.

Whatever was the precise mechanism for thinning the northern crust and generating the extensive lava flows that later covered the entire region, it is apparent that this process effectively reduced the number and intensity of crustal magnetic anomalies. If the subcrustal erosion hypothesis is assumed to be valid, then it is possible that many anomaly sources were located in the preexisting lower crust that was later eroded away. The subsequent extensive volcanic lava flows may also have masked or thermally demagnetized surficial anomaly sources. If some form of the impact hypothesis for the dichotomy is instead assumed to be valid, then the relative absence of magnetic anomalies in the northern lowlands may be a consequence of impact destruction of anomaly sources. In support of the latter hypothesis, the relative dearth of crustal anomalies near the

Hellas and Argyre basins [Acuña *et al.*, 1999, 2001] indicates that shock and heat associated with these basin-forming impacts was sufficient to destroy most preexisting crustal magnetization in these regions. However, it is equally possible that the reduction in number and amplitudes of anomalies in the northern polar region had a different (internal, tectonic) origin. In either case the northern polar anomalies studied here must represent exceptional regions that escaped the destructive processes that eliminated most anomalies in the northern polar zone.

In view of the lack of geologic constraints on source body dimensions, only approximate bounds on bulk magnetization intensities within these sources can be estimated on the basis of the modeling results of the previous section. Such limits may then be useful for ultimately identifying likely magnetic phases. One additional constraint on source body geometry is that magnetization can be preserved in Martian crustal rocks only at depths less than that of the Curie isotherm (853 K for magnetite). According to Banerdt *et al.* [1992], lithospheric thermal gradients at the times when surface loads were emplaced on Mars were in the range of 5-15 K/km; this range is based on tectonic studies of elastic lithosphere thickness combined with laboratory rheological measurements on rocks. The implied Curie depths for magnetite are in the range of ~40-120 km. Thus the northern and southern anomaly sources must be at shallower depths than this. In addition, assuming that subsurface mass variations are a consequence of variations in the thickness of a constant-density crust, Zuber *et al.* [2000] have applied MGS topography and gravity data to infer an approximately uniform thickness of ~35-40 km for the crust under the northern lowlands. This result also suggests relatively shallow depths for the anomaly sources studied here.

The point dipole modeling results of the previous section yielded source depths of >150 km for both the northern and southern anomalies. These depths are significantly larger than likely Curie isotherm or lower crustal boundary depths; for this reason, the point dipole source model appears unlikely. In the remainder of this section we therefore consider only the results assuming a source model consisting of a circular disk of unknown thickness t , dipole moment per unit area m /area, and diameter D located near the surface.

Lower limits on bulk magnetization intensity for the sources of the northern polar anomalies may be estimated from the surface disk results of dipole moment per unit area combined with upper limits on the source thickness. Taking an upper bound of $t \simeq 100$ km, one obtains minimum magnetization intensities of ~0.4 A/m (4×10^{-4} G) and ~0.9 A/m (9×10^{-4} G) for the northern and southern anomalies, respectively. Assuming a nominal mass density of ~3000 kg/m³, the specific minimum magnetization intensities are about

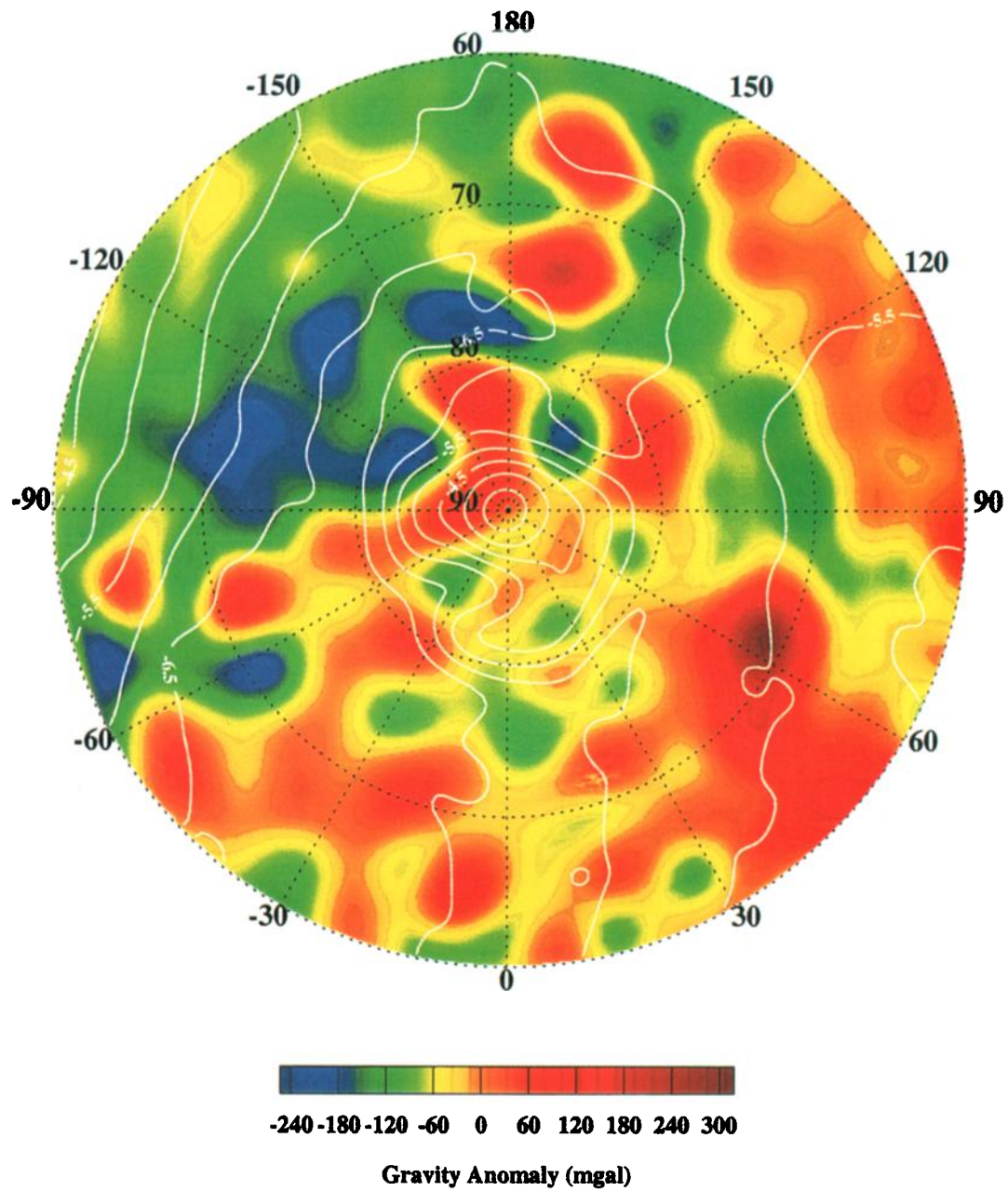


Plate 2. Bouguer (topography-corrected) gravity anomaly map of the north polar zone (60°N to 90°N) based on MGS Doppler gravity data (A. Konopliv, private communication, 2000). Contours of topography (in kilometers) are drawn on the basis of Mars Orbiter Laser Altimeter data [Smith *et al.*, 1999].

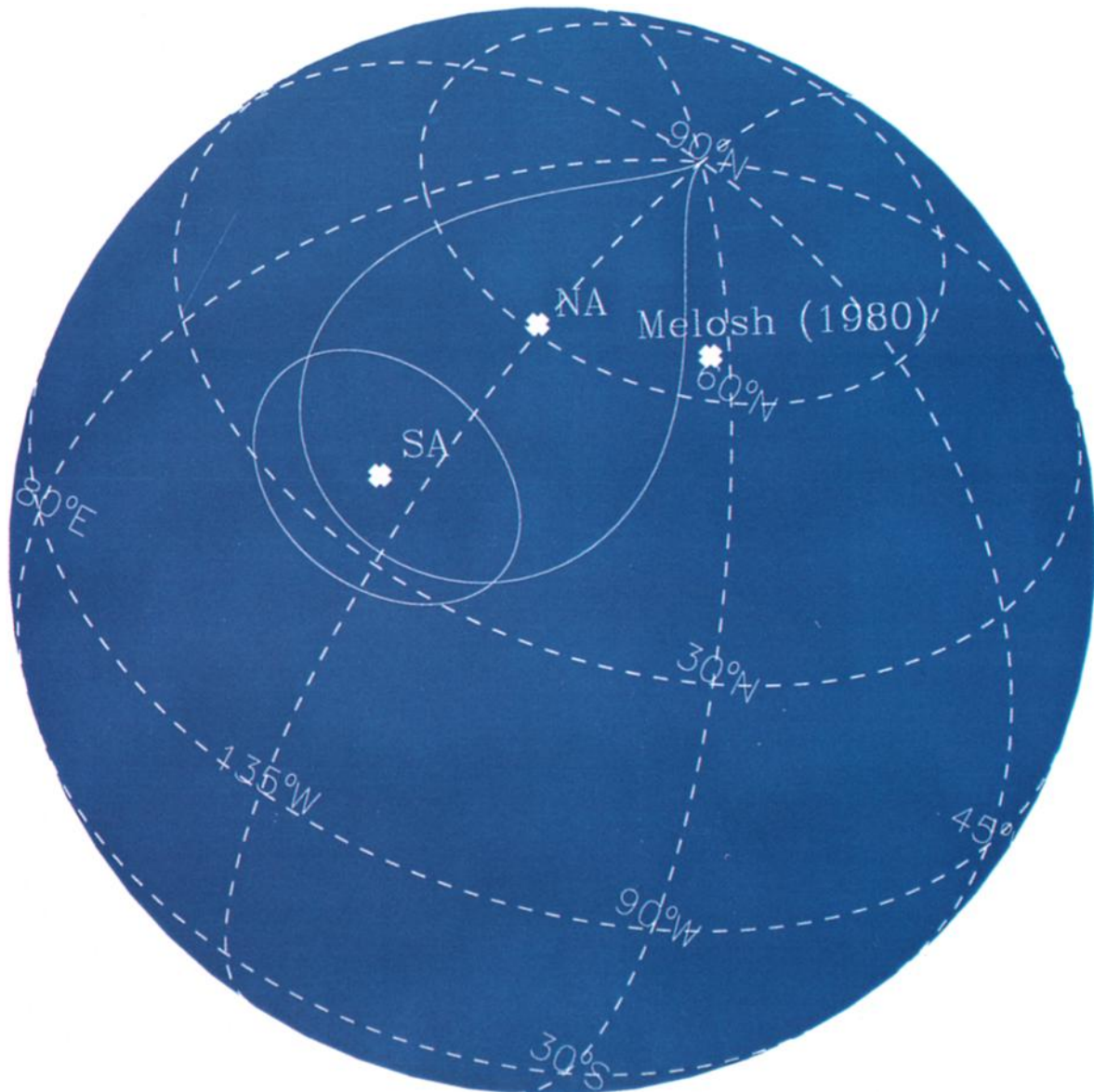


Plate 3. South paleomagnetic pole positions corresponding to the inferred bulk directions of magnetization for the southern and northern anomalies of Plate 1. Approximate error ellipses are calculated using methods given in the text. Also indicated is the location of the paleopole estimated theoretically by *Melosh* [1980] prior to a hypothesized reorientation of the planet at the time of the formation of the Tharsis gravity anomaly.

$1.3 - 3.0 \times 10^{-4} \text{ Am}^2/\text{kg}$ ($= 1.3 - 3.0 \times 10^{-4} \text{ emu/gm}$). Actual magnetization intensities could easily be >1 order of magnitude larger than this if the source thicknesses are much less and/or if the magnetization intensity is variable within the source.

Currently, the only samples of Martian crustal materials that have been directly studied are the SNC meteorites. Like terrestrial basalts, SNC meteorites contain titanomagnetite as a primary magnetic phase; these samples apparently acquired their primary remanence in the presence of a paleofield of amplitude $1 - 10 \mu\text{T}$ [Collinson, 1986; Cisowski, 1986]. After elimination of samples showing evidence for contamination by the terrestrial field during atmospheric entry, bulk magnetization intensities for shergottites and nakhlites are in the range of $1 - 6 \times 10^{-5} \text{ Am}^2/\text{kg}$ ($= 1 - 6 \times 10^{-5} \text{ emu/gm}$) [Collinson, 1986; Cisowski, 1986]. This measured range is significantly less than the minimum magnetization intensities ($> 10^{-4} \text{ Am}^2/\text{kg}$) inferred for the sources of the northern and southern anomalies of Plate 1. In addition, Connerney *et al.* [1999] have recently estimated even larger magnetization intensities ($\sim 10^{-2} \text{ Am}^2/\text{kg}$ or $\sim 10^{-2} \text{ emu/gm}$) for some higher-amplitude southern hemisphere anomaly sources. Rocks containing substantially larger concentrations of titanomagnetite than SNC meteorites, or magnetic phases in addition to titanomagnetite, are therefore probably needed to explain the amplitudes of Martian magnetic anomalies. (For general overviews of terrestrial magnetic petrology, see Clark [1997, 1999].) Furthermore, the SNC meteorites studied by Collinson and Cisowski have low to moderate specific susceptibilities ($0.5 - 3.5 \times 10^{-6} \text{ m}^3/\text{kg}$ for Collinson's samples; generally $\sim 40 \times 10^{-6} \text{ m}^3/\text{kg}$ for Cisowski's samples), indicating titanomagnetite contents of $\sim 0.04 - 0.3\%$ by volume and $\sim 4\%$ by volume, respectively. If the sources of Martian anomalies are composed of material similar to the SNC meteorites, but acquired remanence in stronger fields than inferred by these authors, comparable to the present geomagnetic field ($\sim 50 \mu\text{T}$), then magnetizations $5 - 50$ times greater than the natural remanent magnetizations (NRM) of the SNC meteorites could be explained. This may require formation of the anomaly sources studied here earlier than the SNC meteorites, when the core dynamo was stronger. In summary, some combination of larger concentrations of magnetic phases and a stronger core dynamo field than inferred for the time of formation of SNC meteorite samples is probably required to explain the large magnetization intensities of Martian orbital anomaly sources.

In this regard, Ozdemir [2000] has recently noted evidence from MGS Thermal Emission Spectrometer data and Mars Pathfinder imaging data for crystalline hematite of possible hydrothermal origin as well as maghemite. Both of these minerals are low-temperature oxidation or weathering products of magnetite and titanomagnetite. Deposition of substantial quantities of hydrothermal hematite could lead to chemical rema-

nant magnetization (CRM) with high intensities [Clark, 1997; Ozdemir, 2000]. Also, Nazarova and Harrison [2000] note that some of the observed anomalies are located in regions where surface water may have existed in middle Mars history [e.g., Head *et al.*, 1999]. They point out that serpentinization of upper mantle rocks on Earth is a hydrothermal process that produces magnetite and leads to CRM. Either of these hydrothermal alteration processes would produce substantial increases in natural remanent magnetization intensities as would be necessary to explain the high amplitudes of Martian magnetic anomalies. Weitz and Rutherford [1999] further point out that Martian basalts with compositions similar to the SNC meteorites and the parent melts of the cumulate SNC rocks would crystallize abundant titanomagnetite, provided conditions were sufficiently oxidized. Interaction of basaltic magma with oxidized surface rocks or with near-surface ice or water, early in Martian history, might account for enhanced titanomagnetite concentrations.

With respect to the time period during which the magnetic anomaly sources studied here formed, it appears that their formation most probably predated the immediate end of the heavy bombardment (upper Hesperian) period. This inference follows from the fact that the north polar plains unit (Vastitas Borealis) over which the southern anomaly is situated is upper Hesperian in age [Tanaka and Scott, 1987]. However, the Martian dynamo may have continued to operate well beyond the upper Hesperian period. This is because, as discussed above, the conditions under which strong crustal anomaly sources formed are not well understood. If conditions favoring the formation of crustal regions containing enhanced concentrations of efficient remanence carriers existed mainly during pre-Hesperian times, then strong magnetic anomaly sources would also date from those times even if the core dynamo continued to operate afterward. For example, if Noachian basalts crystallized abundant titanomagnetite because of more oxidizing conditions at that time, then Martian magnetic anomalies would date mainly from the Noachian epoch even if the dynamo continued to operate during Hesperian and later times.

By a similar line of reasoning, the absence of strong magnetic anomalies over the Tharsis volcanic constructs [Acuña *et al.*, 1999, 2001] does not necessarily imply that the dynamo must have ceased operation prior to the formation of Tharsis. If subsurface volcanic deposits in the Tharsis region are magnetized at levels comparable to those of the SNC meteorites, maximum field magnitudes at 300 km altitude would be in the range of $1 - 5 \text{ nT}$ and would therefore be difficult to detect with the MGS magnetometer [Hood and Hartdegen, 1997]. As shown above, much stronger magnetization levels are necessary to explain the northern polar anomalies, and these levels may have been realized only when large concentrations of titanomagnetite or other remanence carriers were produced. The Tharsis basalts may not have

yielded such large concentrations of efficient remanence carriers. Similarly, the dearth of anomalies near the Hellas and Argyre impact basins does not necessarily imply that a Martian dynamo did not exist when these basins formed. Even if an ambient field was present during the postimpact cooling period, acquisition of new magnetization may have been limited by the absence of large concentrations of magnetic remanence carriers during this period.

4.2. Paleomagnetic Pole Positions

As noted in the introduction, a significant areographic clustering of paleomagnetic pole positions estimated for relatively isolated Martian magnetic anomalies would (1) add support to the core dynamo hypothesis for the origin of Martian paleomagnetism and (2) provide a means of investigating past orientations of the rotational pole with respect to the planet. The south magnetic pole positions estimated in section 3 for the two northern polar anomalies analyzed here are plotted in Plate 3 together with the corresponding error ellipses. (Since dynamo reversals are allowed, it is arbitrary whether the south or the north positions are plotted here.) While additional pole positions are needed to establish statistically a significant clustering, it is of interest that these two positions are in the same general areographic region, i.e., in an area between Olympus Mons and the present rotational north pole. Moreover, as discussed below, it is of interest that this region is roughly near the location expected theoretically for the orientation of the spin axis of Mars prior to the formation of the Tharsis mass anomaly.

Polar wander on Mars associated with the formation of the Tharsis volcanic province and gravity anomaly has previously been discussed and investigated by several authors [Mutch *et al.*, 1976; Melosh, 1980; Willemann, 1984; Banerdt *et al.*, 1992]. Although the rotation axis of a planet remains fixed in space by angular momentum conservation, any process that alters the internal distribution of mass will cause the planet to reorient itself with respect to that axis. The reorientation is such that the axis of the maximum principal moment of inertia becomes aligned with the spin axis, thereby yielding a minimum-energy rotational state. In particular, the addition of excess mass to a planetary surface will tend to reorient the planet such that the mass excess is moved toward the equator. The internal volcanic processes that led to the formation of the very large Tharsis gravity anomaly would therefore have led to such polar wander unless Tharsis coincidentally formed on the rotational equator. For example, if Tharsis had originally formed 30° north of its present location, the rotational pole before the formation of Tharsis should be located near 60°N in the present areographic coordinate system. If Tharsis is represented as a simple point mass on the surface of a rigid sphere, the reorientation would be exactly 30° southward with no change in longitude. In reality, the gravity anomaly distribu-

tion prior to the formation of Tharsis is not precisely known, and other effects (e.g., oblateness of an elastic lithosphere) may have tended to oppose the polar reorientation. Hence the actual polar shift may have been more complex than this.

The most straightforward attempt to estimate the location of the former pole of Mars prior to the formation of the Tharsis region was reported by Melosh [1980]. His approach was to attempt to remove the Tharsis anomaly from the gravity field and recompute the ancient pole position from the remaining gravity anomalies. Specifically, the inertia tensor without the Tharsis anomaly was constructed and diagonalized to estimate the maximum principal moment orientation. Using the gravity model of Sjogren *et al.* [1975], it was found that the removal of the Tharsis anomaly results in a shift of the pole by 25° in latitude to 95°W, 65°N. The location of this theoretically predicted position is indicated in Plate 6. Considering the errors associated with the anomaly modeling of section 3, the theoretical location is in reasonable agreement with the magnetic pole position locations.

As pointed out by Melosh [1980], significant errors are associated with the theoretical pole location. Most important, because of the high amplitude of the Tharsis anomaly compared to other gravity anomalies on Mars, a small error in the residual gravity field would lead to a large error in the predicted pole position. This is especially true since the present gravity anomaly field outside of the Tharsis region is not necessarily equal to the gravity field prior to the formation of Tharsis (including the preexisting field in the Tharsis region, which is unknown). Other error sources include (1) the difficulty of separating the dynamical (liquid behavior) portion of the oblateness coefficient J_2 from the solid body portion that contributes to the moment of inertia; (2) partial isostatic compensation of the Tharsis surface load; and (3) effects on polar stability of an elastic lithosphere. Willemann [1984] attempted to account for the effects of an elastic lithosphere and partial compensation of the Tharsis load. According to his model, the reorientation of Mars at the time of the formation of Tharsis was only 3°–9° in latitude. Most recently, Zuber and Smith [1997] have removed the Tharsis gravity anomaly from the full Mars gravity field and conclude that the formation of Tharsis may have resulted in polar wandering but only if the planet's elastic lithosphere was thin enough to preclude retention of a fossil rotational bulge. No prediction of the paleopole location was given by these authors.

In addition to theoretical estimates of the pre-Tharsis pole position, a number of authors have presented various geologic observations that were proposed as constraints on polar wandering on Mars. For example, Mutch *et al.* [1976] proposed that the presence of furrowed terrain in an approximate circle around Mars tilted by 15° to the equator could represent geologic evidence for planetary reorientation. They argued that

the development of this terrain was controlled by fluvial and meteorological processes that should be symmetric about the ancient equator. On this basis they estimated a paleopole position at 75°N, 110°W. *Melosh* [1980] estimated the fracture patterns expected from a polar reorientation after the formation of Tharsis. However, other tectonic fault processes may have been more dominant because the expected fracture patterns were not recognized except possibly for a north-south trending system north of Tharsis. Later, *Schultz and Lutz* [1988] argued that deposits similar to those presently observed in polar regions are present elsewhere on the planet, including in equatorial regions. On this basis they proposed an extensive history of polar wandering occurring in a series of relatively rapid polar shifts. However, most of the inferred paleopole positions are not near the paleomagnetic pole positions of Plate 3. Also, other explanations for the origins of some of the equatorial deposits have been suggested [*Scott and Tanaka*, 1982; *Greeley and Guest*, 1987].

5. Conclusions

Although more detailed mapping and modeling of the two northern polar magnetic anomalies considered here should be performed in the future, the results of sections 2 and 3 and the interpretational analysis of section 4 permit the following provisional conclusions to be drawn:

1. Most of the northern polar lowland region is magnetically weak in comparison to the southern highlands mapped earlier by the MGS magnetometer [*Acuña et al.*, 1999]. This relative absence of strong crustal magnetization is probably a consequence of the process (e.g., tectonic subcrustal erosion) that was responsible for thinning the northern crust and generating the extensive lava flows that cover the region.

2. The sources of the northern polar anomalies studied here formed prior to the immediate end of the heavy bombardment (upper Hesperian) period. Considering likely maximum depths to the Curie isotherm at the time of magnetization acquisition, minimum magnetization intensities for the sources of the north polar anomalies are conservatively in the range of $1.3 - 3.0 \times 10^{-4}$ Am²/kg (or emu/gm). These intensities appear to require enhanced titanomagnetite concentrations and/or magnetic phases in addition to titanomagnetite in igneous materials. Enhanced titanomagnetite concentrations in more oxidized igneous rocks, plus a relatively strong paleofield during early Martian history, could account for these inferred magnetization intensities.

3. These results imply that a former Mars core dynamo existed prior to the upper Hesperian period. Without further knowledge about formation mechanisms for anomaly sources, no definite constraints can be imposed on the time of cessation of the Mars core dynamo.

4. The paleomagnetic pole positions corresponding to the bulk directions of magnetization inferred for the northern polar anomaly sources both lie in a region north of Olympus Mons and south of the present rotational pole. This region is centered on approximately 50°N, 135°W and is not greatly distant from the location (65°N, 95°W) estimated theoretically by *Melosh* [1980] for the paleopole prior to the formation of the Tharsis volcanic province and gravity anomaly.

Acknowledgments. Supported by the NASA Mars Data Analysis program under grant NAG5-8185. The authors thank David Clark of CSIRO Exploration and Mining for a constructive critical review. Helpful critical comments by G. Schubert, H. J. Melosh, and J. C. Cain are also gratefully acknowledged. Plate 2 was generously provided by Alex Konopliv and Dah-Ning Yuan.

References

- Acuña, M., et al., Magnetic field and plasma observations at Mars: Initial results of the Mars Global Surveyor mission, *Science*, **279**, 1676-1680, 1998.
- Acuña, M., et al., Global distribution of crustal magnetization discovered by the Mars Global Surveyor MAG/ER experiment, *Science*, **284**, 790-793, 1999.
- Acuña, M., et al., Magnetic field of Mars: Summary of results from the aerobraking and mapping orbits, *J. Geophys. Res.*, in press, 2001.
- Banerdt, B., M. P. Golombek, and K. L. Tanaka, Stress and tectonics on Mars, in *Mars*, edited by H. Kieffer et al., pp. 249-297, Univ. of Ariz. Press, Tucson, 1992.
- Butler, R. F., *Paleomagnetism: Magnetic Domains to Geologic Terranes*, 319 pp., Blackwell Sci., Malden, Mass., 1992.
- Cisowski, S. M., Magnetic studies on Shergotty and other SNC meteorites, *Geochim. Cosmochim. Acta*, **50**, 1043-1048, 1986.
- Clark, D. A., Magnetic petrophysics and magnetic petrology: Aids to geological interpretation of magnetic surveys, *AGSO J. Aust. Geol. Geophys.*, **17**, 83-103, 1997.
- Clark, D. A., Magnetic petrology of igneous intrusions: Implications for exploration and magnetic interpretation, *Explor. Geophys.*, **30**, 5-26, 1999.
- Collinson, D. W., Magnetic properties of Antarctic shergottite meteorites EETA 79001 and ALHA 77005: Possible relevance to a Martian magnetic field, *Earth Planet. Sci. Lett.*, **77**, 159-164, 1986.
- Connerney, J. E. P., M. Acuña, P. Wasilewski, N. Ness, H. Rème, C. Mazelle, D. Vignes, R. Lin, D. Mitchell, and P. Cloutier, Magnetic lineations in the ancient crust of Mars, *Science*, **284**, 794-798, 1999.
- Eliason, E. M., and L. A. Soderblom, An array processing system for lunar geochemical and geophysical data, *Proc. Lunar Sci. Conf. 8th*, 1163-1170, 1977.
- Frey, H., and R. Schultz, Large impact basins and the megaimpact origin for the crustal dichotomy on Mars, *Geophys. Res. Lett.*, **15**, 229-232, 1988.
- Fuller, M. and S. Cisowski, Lunar paleomagnetism, in *Geomagnetism*, vol. 2, edited by J. A. Jacobs, pp. 307-456, Academic, San Diego, Calif., 1987.
- Greeley, R., and J. Guest, Geologic map of the eastern equatorial region of Mars, *U.S. Geol. Surv. Misc. Invest. Ser., Map I-1802-B*, 1987.
- Hargraves, R. B., D. W. Collinson, R. E. Arvidson, and C. R. Spitzer, The Viking magnetic properties experiment:

- Primary mission results, *J. Geophys. Res.*, *82*, 4547-4558, 1977.
- Head, J. W., III, H. Hiesinger, M. Ivanov, M. Kreslavsky, S. Pratt, and B. Thomson, Possible ancient oceans on Mars: Evidence from Mars Orbiter Laser Altimeter data, *Science*, *286*, 2134-2137, 1999.
- Hide, R., Comments on the Moon's magnetism, *Moon*, *4*, 39, 1972.
- Hood, L. L., Bulk magnetization properties of the Fra Mauro and Reiner Gamma Formations, *Proc. Lunar Planet. Sci. Conf. 11th*, 1879-1896, 1980.
- Hood, L. L., Frozen fields, *Earth Moon Planets*, *67*, 131-142, 1995.
- Hood, L. L., and K. Hartdegen, A crustal magnetization model for the magnetic field of Mars: A preliminary study of the Tharsis region, *Geophys. Res. Lett.*, *24*, 727-730, 1997.
- Hood, L. L., and A. Vickery, Generation of transient magnetic fields in hypervelocity meteoroid impacts with application to lunar paleomagnetism, *Proc. Lunar Planet. Sci. Conf. 15th*, Part 1, *J. Geophys. Res.*, *89*, suppl. C211-C223, 1984.
- Hood, L., C. Russell, and P. Coleman Jr., Contour maps of lunar remanent magnetic fields, *J. Geophys. Res.*, *86*, 1055-1069, 1981.
- Hood, L., A. Zakharian, J. Halekas, D. Mitchell, R. Lin, M. Acuña, and A. Binder, Initial mapping and interpretation of lunar crustal magnetic anomalies using Lunar Prospector magnetometer data, *J. Geophys. Res.*, in press, 2001.
- Langel, R., and W. Hinze, *The Magnetic Field of the Earth's Lithosphere: The Satellite Perspective*, 429 pp., Cambridge Univ. Press, New York, 1998.
- McGill, G., and A. Dimitriou, Origin of the Martian global dichotomy by crustal thinning in the late Noachian or early Hesperian, *J. Geophys. Res.*, *95*, 12,595-12,605, 1990.
- Melosh, H. J., Tectonic patterns on a reoriented planet, *Icarus*, *44*, 745-751, 1980.
- Mutch, T., R. Arvidson, A. Binder, E. Guinness, and E. Morris, *The Geology of Mars*, Princeton Univ. Press, Princeton, N. J., 1976.
- Nazarova, K. A., and C. G. A. Harrison, Serpentinization of Martian crust and mantle and the nature of Martian magnetic anomalies, *Eos Trans. AGU*, *81*(19), Spring Meet. Suppl., S173, 2000.
- Nimmo, F., and D. J. Stevenson, Influence of early plate tectonics on the thermal evolution and magnetic field of Mars, *J. Geophys. Res.*, *105*, 11,969-11,979, 2000.
- Ozdemir, O., Chemical remanent magnetization - Possible source of the magnetization of Martian crust?, *Eos Trans. AGU*, *81*(19), Spring Meet. Suppl., S173, 2000.
- Russell, C. T., Planetary magnetism, in *Geomagnetism*, vol. 2, edited by J. A. Jacobs, pp. 458-523, Academic, San Diego, Calif., 1987.
- Schubert, G., and T. Spohn, Thermal history of Mars and the sulfur content of its core, *J. Geophys. Res.*, *95*, 14,095-14,104, 1990.
- Schultz, P. H., and A. Lutz, Polar wandering of Mars, *Icarus*, *73*, 91-141, 1988.
- Scott, D. H., and K. Tanaka, Ignimbrites of Amazonis Planitia region of Mars, *J. Geophys. Res.*, *87*, 1179-1190, 1982.
- Sjogren, W., J. Lorell, L. Wong, and W. Downs, Mars gravity field based on a short arc technique, *J. Geophys. Res.*, *80*, 2899-2908, 1975.
- Smith, D., et al., The global topography of Mars and implications for surface evolution, *Science*, *284*, 1491-1503, 1999.
- Stevenson, D. J., T. Spohn, and G. Schubert, Magnetism and thermal evolution of the terrestrial planets, *Icarus*, *54*, 466-489, 1983.
- Strom, R., S. Croft, and N. Barlow, The Martian impact cratering record, in *Mars*, edited by H. Kieffer et al., pp. 383-423, Univ. of Ariz. Press, Tucson, 1992.
- Tanaka, K., and D. Scott, Geologic map of the polar regions of Mars, scale 1:15,000,000, *U.S. Geol. Surv. Misc. Invest. Ser., Map I-1802-C*, 1987.
- Tanaka, K., D. Scott, and R. Greeley, Global stratigraphy, in *Mars*, edited by H. Kieffer et al., pp. 345-382, Univ. of Ariz. Press, Tucson, 1992.
- Weitz, C. M., and M. J. Rutherford, Petrological explanation for the magnetic anomalies detected on Mars, paper presented at Fifth International Conference on Mars, Calif. Inst. of Technol., Pasadena, Calif., 1999.
- Wilhelms, D., and S. Squyres, The Martian hemispheric dichotomy may be due to a giant impact, *Nature*, *309*, 138-140, 1984.
- Willemann, R. J., Reorientation of planets with elastic lithospheres, *Icarus*, *60*, 701-709, 1984.
- Wise, D. U., M. Golombek, and G. McGill, Tectonic evolution of Mars, *J. Geophys. Res.*, *84*, 7934-7939, 1979.
- Zuber, M., and D. Smith, Mars without Tharsis, *J. Geophys. Res.*, *102*, 28,673-28,685, 1997.
- Zuber, M., et al., Internal structure and early thermal evolution of Mars from Mars Global Surveyor topography and gravity, *Science*, *287*, 1788-1793, 2000.

L.L. Hood and A. Zakharian, Lunar and Planetary Laboratory, University of Arizona, Kuiper Space Sciences Building, 1629 East University Boulevard, Tucson, AZ 85721-0092. (lon@lpl.arizona.edu)

(Received June 27, 2000; revised February 9, 2001; accepted February 13, 2001.)